A Polycation-Modified Nanofillers Tailored Polymer Electrolytes Fiber for Versatile Biomechanical Energy Harvesting and Full-Range Personal Healthcare Sensing

Zihua Li[1], Bingang Xu[1,], Jing Han[1], Junxian Huang[1], Hong Fu[2]*

[1]Research Institute of Intelligent Wearable Systems, Institute of Textiles and Clothing, The Hong Kong Polytechnic University, 999077, Hong Kong

[2]Department of Mathematics and Information Technology, The Education University of Hong Kong, 999077, Hong Kong

*Corresponding author. E-mail address: tcxubg@polyu.edu.hk (B. Xu).

Abstract:

The emergence of fibrous energy harvesters and self-powered sensors gives birth to functional wearable electronics. However, low power outputs, poor sensing abilities, and limited material selections have greatly restricted their developments. Herein, novel polycation-modified carbon dots (PCDs) tailored PCDs/polyvinyl alcohol nanocomposite polymer electrolytes (NPEs) are prepared and used as dominating triboelectric materials to construct a new NPEs-based fiber triboelectric nanogenerator (NPE-TENG) for the first time. The filling of PCDs endows NPEs with enhanced ionic conductivity. The developed NPE-TENG can respond to different mechanical stimuli with excellent flexibility and deliver a high power density of 265.8 $\mu W\ m^{-1}$. Self-powered wearable sensor and smart glove based on NPE-TENG are further developed, which can achieve skin-level tactile sensing and joint-related activities monitoring in a rapid, real-time, and non-invasive way. As a sustainable power source, the NPE-TENG can drive small electronics and light up hundreds of LEDs. This work not only renders new insights into the development of triboelectric materials for fiber-based TENG, but also provides a direction for potential applications of fibrous biomechanical energy harvesters and self-powered sensors in wearable electronics, personal healthcare monitoring, and human-machine interactions.

Keywords: polymer electrolyte, fiber, triboelectric nanogenerator, self-powered wearable sensor

1. Introduction

Wearable electronics are rapidly flourishing in various fields including artificial intelligence, human-machine interaction, personal healthcare monitoring, etc.[1-4] An urgent problem emerged behind this prosperity is that multifunctional wearable electronics are highly desired to resolve the limited lifespan, periodic charging, potential safety hazards, and unsustainable issues during heavy usage of conventional energy storage units.[5-9] Techniques that can harvest energy from surroundings and generate electricity directly are highly promising to address these issues, such as solar cells,[10-12] thermoelectric generators,[13, 14] biofuel cells,[15, 16] and triboelectric nanogenerators (TENGs).[17, 18] Among them, TENGs based on a coupling effect of triboelectrification and electrostatic induction can convert ubiquitous, neglected, and low-frequency biomechanical energy into electricity. It has huge application potential in wearable powering,[19] multifunctional self-powered sening[20, 21] and healthcare monitoring[22, 23] owing to its outstanding virtues of low cost, high conversion efficiency, environmental friendliness, and easy availability. However, the development of traditional TENGs with a planar construction has limitations in the fields of wearable electronics due to their restricted deformability and clothing aesthetics. In contrast, fiber-based TENG can be readily integrated into conventional textiles, resulting in more possibilities for wearable power supplies and self-powered sensors because of its merits of compactness, versatile deformability, breathability, and washability.[24-27]

Nevertheless, fiber-based TENG is facing the development dilemmas of low power

outputs, poor sensing capabilities, and limited selections of triboelectric materials.[24, 28] These inherent issues restrain developments and applications of wearable energy harvesters and self-powered sensors. Some works on the geometry design have been carried out to address these issues. For instance, Dong et al. reported a three-dimensional five-directional braided structural TENG and achieved a versatile e-textile with enhanced power output and pressure sensitivity.[29] Han et al. developed a multifunctional coaxial energy fiber composed of TENG, supercapacitor and pressure sensor, and this energy fiber presented acceptable power output and good sensitivity of finger motions.[30] Ning et al. developed a highly flexible and stretchable coaxial structural TENG which was used as a tactile sensor to respond to versatile mechanical stimuli.[31] Although these fiber-based TENGs show good electrical performance and sensing abilities, their further developments may be subject to confined material selections.

Recently, inorganic salts doped solid polymer electrolytes (SPEs) have been verified to be an effective way to manipulate the triboelectricity of materials.[32-35] For example, incorporating calcium chloride into polyvinyl alcohol (PVA) can achieve a significantly enhanced triboelectric performance.[32] However, the addition of inorganic salts into polymers may sacrifice mechanical properties due to the poor interfacial compatibility between the polymer matrix and large-grained inorganic dopants.[36] In addition, the high hygroscopicity and poor dispersibility of inorganic salts may also bring challenges in the further development of this kind of polymer electrolytes in TENG techniques.

Adding functionalized nanofillers into polymer matrixes is a proven effective strategy to enhance the dielectricity of composites without sacrificing mechanical properties and dispersibility.[37-39] Particularly, carbon dots (CDs) enriched with oxygen-containing functional groups are ideal nanofillers for fabricating functionalized SPEs owing to their good dispersion and ultrafine particles.[40, 41] When the size of nanofillers reduces to dozens of nanometers, a positive impact on the ionic conductivity of SPEs will occur,[42] which is not available for large-grained inorganic salts doped SPEs. Even so, fabrication of CDs-based SPEs fibers for TENGs have not been reported.

With these considerations, we fabricated a novel nanocomposite polymer electrolytes (NPEs) by incorporating polycation-modified CDs (PCDs) into the PVA matrix and developed a novel type of NPEs fiber, namely NPEs coated conductive silver-plated nylon yarns (NPE@SPNYs). The introduction of PCDs can significantly improve the triboelectric performance of NPEs fiber by enhancing the ionic conductivity, which is essentially different from inorganic salts-doped SPEs. Based on the NPEs fiber, a kind of core-sheath fiber TENG (NPE-TENG) was further developed for efficient biomechanical energy harvesting and versatile full-range personal healthcare monitoring, in which the NPE@SPNYs dielectric core is the dominating triboelectric material. The developed NPE-TENG could rapidly respond to various mechanical stimuli and effectively convert mechnical energy into electric energy with a maximum peak power density of 265.8 $\mu W\ m^{-1}$ and reliable durability of 30,000 testing cycles. On the base of NPE-TENG, a self-powered wearable sensor was developed and could

realize the full-range personal healthcare sensing from physiological signals (subtle expression, respiration, and vocal-cord vibration) to joint motions (wrist, elbow, and knee) in a rapid, real-time, and noninvasive way. In addition, a self-powered smart glove was also designed for gestures detection and recognition. As a power source, the NPE-TENG can charge commercial capacitors, drive small electronics, and light up hundreds of LEDs. Hence, the developed NPE-TENG with high power output, good sensitivity and full-range detection demonstrates wide application potential in wearable powering and personal healthcare monitoring.

2. Result and discussion

PCDs were facilely synthesized by a microwave-assisted pyrolytic reaction in the presence of citric acid, urea, and polyethyleneimine (PEI) (Fig. 1a). To confirm the pre-synthesized products, chemical components of PCDs were investigated firstly. Fourier transform infrared (FTIR) spectra show that pure PEI has the stretching vibration of N–H and C–H at 3500 – 3100 cm^{-1} and 2900 – 2700 cm^{-1}, bending absorption of N–H at 1650 – 1580 cm^{-1} and C–H at 1460 cm^{-1}, and stretching absorption of C–N at 1340 – 1020 cm^{-1}, respectively (Fig. S1). They are kept well in the FTIR spectrum of the as-prepared PCDs, indicating the grafting of PEI groups on the surface of PCDs.[43] X-ray photoelectron spectroscopy (XPS) spectra verify that atomic ratios of C, N, and O in PCDs are 71.63%, 5.54%, and 22.83%, respectively (Fig. S2a). The deconvolution of C1s shows four peaks at 284.6, 285.7, 287.9, and 288.9 eV, corresponding to C–C/C=C, C–N/C–O, C=N/C=O, and O=C–OH, respectively (Fig. S2b). The N1s signal generates

three peaks with respect to pyridinic N at 399.2 eV, pyrrolic N at 400.1 eV, and graphitic N at 401.5 eV, respectively (Fig. S2c), revealing the existence of both dopant-N atoms (C–N–C, N–$(C)_3$) and amide–N (N–H) moieties.[44] The O1s spectrum shows two fitted peaks at 532.0 and 532.9 eV, which are associated with C=O and C–O–C/C–O–H (Fig. S2d). These results show PEI as functional groups are successfully introduced on the surface of carbon dots. Thanks to the presence of polycationic PEI moieties, PCDs are ideal polymer electrolyte nanofillers that can dissociate into fixed charged polymer chains and draw mobile ions upon hydrating (Fig. 1a).[40, 41] Moreover, the morphologies and size of PCDs were also investigated. Atomic force microscopy (AFM) image shows that PCDs have good uniformity and spherical structure (Fig. 1b) with an ultrafine average size of ~ 1.59 nm (Fig. S3). The results were further confirmed by transmission electron microscopy (TEM) images of PCDs (Fig. S4). In addition, X-ray diffraction (XRD) pattern reveals that PCDs have good crystallization properties (Fig. S5).

Owing to the ultrafine size and abundant oxygen-containing functional groups, PCDs have good water solubility and are highly suitable as functional nanofillers for preparing PCDs/PVA-based NPEs (Fig. S6). The NPEs can be readily obtained by blending PCDs and PVA aqueous solution owing to its good water solubility and multiple interfacial polarization caused by ultrafine PCDs. The as-prepared NPEs exhibit uniform brownish gels in aqueous solution, indicating excellent processability (Fig. 1c and S7). Rich amorphous regions and abundant –OH groups of PVA may

provide an appropriate matrix to dissolve polycationic amino on the surface of PCDs, and thus achieve high dielectric property and ionic conductivity (Fig. 1d).[34] Electrochemical impedance spectroscopy (EIS) was employed to evaluate the ionic conductivities of NPEs with different amounts of PCDs (Fig. S8). As shown in Fig. 1e, with increase of PCDs from 1 to 5 wt%, the charge-transfer resistance (R_{ct}) of NPEs is decreased from 10.35 to 4.56 kΩ and is much smaller than that of pristine PVA (13.80 kΩ). This is mainly due to the high charge mobility caused by the reliable polycationic doping effect in NPEs.[40, 41] The ionic conductivities (σ, S cm^{-1}) of NPEs were further determined from EIS spectra. It can be calculated by $\sigma = d/R_bA$, where, d (cm), R_b (Ω), and A (cm^2) represent thickness, bulk resistance, and effective area of the measured sample, respectively. As shown in Fig. 1f, NPEs present an enhanced ionic conductivity from 1.02×10^{-7} to 2.33×10^{-7} S cm^{-1} as the concentration of PCDs increases from 1 to 5 wt%, which is much higher than that of the pristine PVA (7.68×10^{-8} S cm^{-1}). After incorporating PCDs into the PVA matrix, the diversity and quantity of hydrophilic moieties are further improved, realizing a high water retention capacity of NPEs. More importantly, as a kind of solid polyelectrolyte, NPEs can dissociate into protonated amine groups ($–NH_3^+$) and attract mobile ions upon hydrating,[45] and thereby enhance their ionic conductivities. Although NPEs remain the relatively low ionic conductivity as compared with conventional SPEs used in batteries,[46] it may be very suitable dielectric materials for TENG owing to the opportune charge mobility.

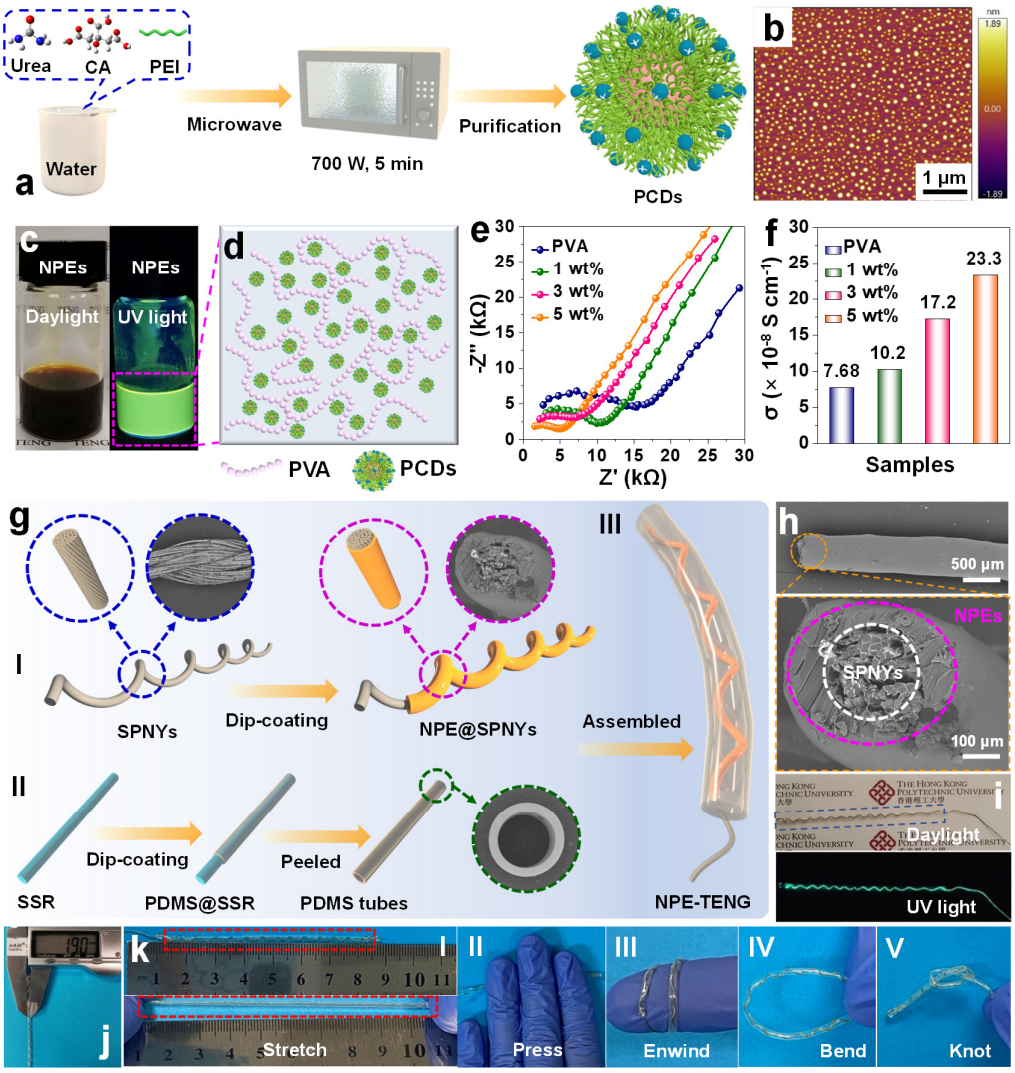

Fig. 1. Synthesis and preparation of PCDs, NPEs, and NPE-TENG. (a) The synthesis route of PCDs. (b) AFM image of PCDs. (c) Photographs of NPEs under daylight and UV illumination (365 nm). (d) Schematic illustration of interactions between PVA and PCDs in NPEs. (e) Nyquist plots, and (f) ionic conductivities of pristine PVA and NPEs with different content of PCDs. (g) Fabrication routes of NPE-TENG. (h) Surface and cross-section SEM images of NPE@SPNYs. (i) Photographs of NPE-TENG under daylight and UV illumination (365 nm). (j) The diameter of NPE-TENG. (k) Photographs of NPE-TENG under diverse mechanical deformations.

Apart from material design, rational constructions of TENG also play a crucial role in

the improvement of its entire properties. It is well known that sufficient contact-separation operating space is highly essential for TENG. Considering all these factors, a highly flexible core-sheath TENG based on helical PCDs/PVA NPEs fiber (NPE-TENG) was designed and developed. Fig. 1g displays fabrication procedure of the core-sheath NPE-TENG. The NPE-TENG could be assembled from a helical dielectric core as the triboelectric material and a PDMS sheath as counterpart and encapsulating materials, in which the helical NPE@SPNYs dielectric core is axially inserted into the PDMS sheath (Fig. 1g-III). The NPE@SPNYs dielectric core was fabricated by coating NPEs on SPNYs and molded in an 80 °C oven, repeatedly (Fig. 1g-I). Compared with bare SPNYs (Fig. S9), NPE@SPNYs with a diameter of ~ 500 μm has a smooth and continuous coating surface (Fig. 1h). The cross-section SEM image presents the NPEs coating layer is densely wrapped on the surface of SPNYs, and the thickness is around 75 μm (Fig. 1h). The PDMS sheath could be easily obtained by dip-coating PDMS solution onto stainless steel rod (SSR) (Fig. 1g-II and S10). As shown in Fig. 1i, the assembled configuration of NPE-TENG composed of the inner helical NPE@SPNYs and the outer transparent PDMS sheath can be displayed clearly under daylight and UV light. The assembled NPE-TENG has a measured diameter of 1.9 ± 0.02 mm (Fig. 1j), which is thinner than most of previous fiber-based TENGs as shown in Table S1.[28-31, 47-51] To confirm its wearability, mechanical deformations of NPE-TENG including stretching (Fig. 1k-I), pressing (Fig. 1k-II), enwinding (Fig. 1k-III), bending (Fig. 1k-IV), and knotting (Fig. 1k-V) were performed. The results indicate that it has good flexibility. To investigate its mechanical properties, the tensile and compression cycling

tests of NPE-TENG were also performed under an applied force. After 10 cycles of tensile and compression, NPE-TENG demonstrates extremely stable mechanical properties (Fig. S11a and b). Then, the stress-strain curve of NPE-TENG was further recorded. Because of the different elastic modulus of NPE@SPNYs core and PDMS sheath, NPE-TENG presents two stages of breaking strain, which are at 151% and 413% of the original length, respectively (Fig. S11c). The mechanical testing results show NPE-TENG has good mechanical robustness and application potential in wearable electronics.

As mentioned above, NPE-TENG can work normally under different mechanical stimuli. Practically, electricity-generating principles of NPE-TENG under various deformation conditions are based on triboelectrification and electrostatic induction. Herein, only the working mechanism of NPE-TENG is illustrated under the compressing operation, and it will work in a single-electrode mode (Fig. 2a). One cycle of compressing and releasing movements is regarded as a complete contact-separation process between PDMS sheath and NPE@SPNYs core. Considering that PDMS has a stronger electron-accepting ability than NPEs, the internal surface of PDMS sheath tends to accumulate negative charges, while NPE@SPNYs core is prone to gather positive charges. At the initial state (Fig. 2a), no charge transfer appears on either side due to the absence of electrical potential difference. When NPE-TENG is compressed, the inner core and the outer sheath will be fully contacted. This process results in generating equivalent charges with opposite polarities at two contact surfaces (Fig. 2b-

I). There is no electrical potential difference between the two surfaces because of the neutralization of two opposite charges. Once the two contact surfaces are separating, negative charges will be induced in the SPNYs electrode owing to the electrostatic induction effect. Meanwhile, the electrical potential difference established between the SPNYs electrode and the ground will promote electrons flow, forming an electric current (Fig. 2b-II). As the device returns to its original state, a new electrical potential equilibrium is achieved, and the electrons stop flowing (Fig. 2b-III). When PDMS sheath approaches NPE@SPNYs core again, electrons move oppositely to balance the electrical potential, resulting in an inverse electric current (Fig. 2b-IV). Hence, the periodic contact-separation process between NPE@SPNYs core and PDMS sheath will generate continuous alternating current outputs.

To investigate the effect of ionic conductivities on the triboelectric performance of NPE-TENG, a set of electrical tests were carried out by changing the content of PCDs added in NPEs under an impact force of 10 N with a frequency of 3 Hz. As the content of PCDs is increased from 0 to 3 wt%, open-circuit voltage (V_{oc}) and short-circuit current (I_{sc}) of NPE-TENG have an obvious enhancement, which is 23.8 V and 0.9 μA, respectively. Then, the V_{oc} and I_{sc} drop to 21.5 V and 0.7 μA as the concentration of PCDs reaches 5 wt% (Fig. S12). As the content of PCDs incorporated into the PVA matrix increases, the surface of NPEs is prone to fix more water molecules and form a water membrane.[52] At relatively high humidity, polycation PEI in NPEs will dissociate into a fixed-charge polymer chain and attract mobile anions (OH^-) on an electrovalent

bond.[45] When NPEs contact with PDMS, the water membrane will provide a transfer channel to help ions transfer from NPEs to PDMS, where transferred charges involve electron transfer and ion transfer during the triboelectrification process.[53] The enhancement of ionic conductivity will facilitate the mobility of mobile ions, resulting in a higher surface charge density and enhanced electrical output. However, NPEs will adsorb excessive water molecules as the content of PCDs increases, which is likely to deteriorate the electrical performance of NPE-TENG due to the accelerated charge dissipation. To confirm this phenomenon, electrical performances of NPEs incorporated with 1 wt% and 3 wt% PCDs were further measured under different relative humidity (RH), respectively. As shown in Fig. S13, the electrical performances of two NPE-TENGs display the same trends with the change of humidity. In a dry condition, two NPE-TENGs show low V_{oc} and short-circuit charge transfer (Q_{sc}), which may be due to the reduction of ionic conductivity caused by the removal of water molecules. When fully exposed to ambient humidity (63% RH), two NPE-TENGs obtain an obvious enhancement in V_{oc} and Q_{sc}, respectively. This is because highly hydrophilic NPEs will fix more water molecules and result in improved ionic conductivity, thereby promoting the mobility of more ions and higher surface charge density. As the humidity increases to 90% RH, the electrical performances of two NPE-TENGs remain almost constant, which may be attributed to the saturation of water molecules immobilized by NPEs. As a result, NPEs incorporated with 3 wt% PCDs are selected for the following study unless otherwise specified.

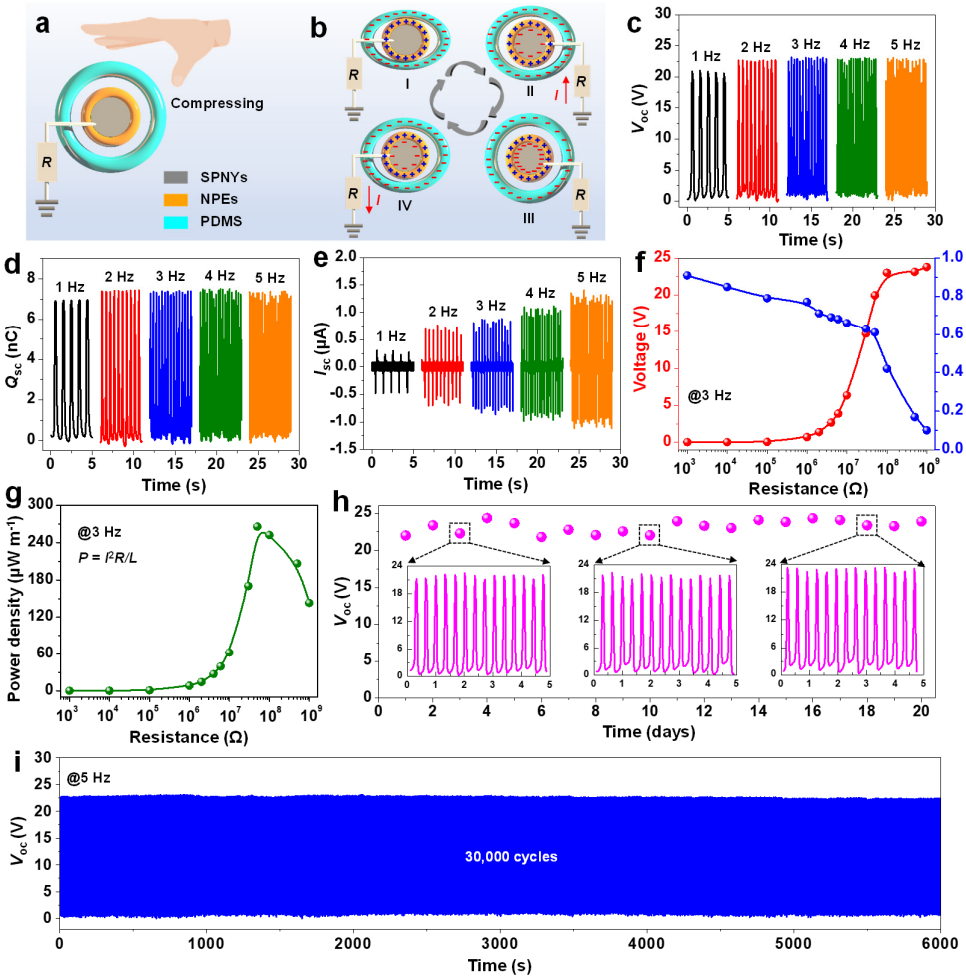

Fig. 2. Working principle and electrical performance of single electrode mode NPE-TENG. (a) and (b) Working principles of NPE-TENG. (c) V_{oc}, (d) Q_{sc} and (e) I_{sc} of NPE-TENG with different frequencies. (f) Output voltage and current, and (g) instantaneous peak power density of NPE-TENG at a series of external loadings. (h) Stability measurement of NPE-TENG for 20 days (Inset: the corresponding real-time V_{oc}). (i) Durability testing of NPE-TENG for continuous 30,000 cycles.

To systematically investigate mechanical energy harvesting properties, electrical outputs of NPE-TENG with a length of 7.0 cm were measured under a compression force of 10 N. As shown in Fig. 2c and 2d, NPE-TENG has an obvious increase in the V_{oc} and Q_{sc} with the increase of frequency from 1 to 2 Hz. It may be attributed to

external electrons flowing to reach equilibrium in a shorter time.[54] Then, the V_{oc} and Q_{sc} of NPE-TENG maintain almost unchanged in the frequency range from 2 to 5 Hz, which is 23.3 V and 7.5 nC, respectively. This interesting phenomenon is consistent with previous reports.[51, 55, 56] While the I_{sc} of NPE-TENG reaches the maximum value of 1.3 μA with the increase of frequency from 1 to 5 Hz (Fig. 2e). The inconsistent variation of electrical outputs as the loading frequency is explained in Supplementary Note S1. Moreover, the V_{oc}, Q_{sc}, and I_{sc} of NPE-TENG were measured at different compression forces at a frequency of 3 Hz (Fig. S14). It can be found that the V_{oc}, Q_{sc}, and I_{sc} show a gradual increase with the increase of force from 1 to 10 N, and then remain constant with the increase of force from 10 to 50 N, as the larger force makes the more contact area between NPE@SPNYs core and PDMS sheath. The power outputs of NPE-TENG were also measured by connecting with a series of external resistances. In Fig. 2f, the output voltage of a single NPE-TENG remains at a minimum value firstly and then rises sharply as resistances increase from 1 kΩ to 1 GΩ. In contrast, the output current of the NPE-TENG decreases gradually with the increase of resistances. In addition, the instantaneous peak power density of the single NPE-TENG was calculated by $P = I^2R/L$, where P, I, R, and L denote power density, output current, external resistance and length of the NPE-TENG, respectively. As shown in Fig. 2g, the instantaneous power density of a single NPE-TENG reaches a peak value of 265.8 μW m^{-1} at an external resistance of 50 MΩ, which is higher than most fiber-based TENGs recently reported (Table S1 and Supplementary Note S2).[28-31, 47-51] Furthermore, the long-term stability of NPE-TENG was presented in Fig. 2h. The result demonstrates

that the V_{oc} of NPE-TENG has no significant decline within 20 days and maintains an average value of 23.2 V, showing good working stability. The durability of NPE-TENG was also measured to estimate its practicability at a frequency of 5 Hz. As shown in Fig. 2i, the V_{oc} remains almost as a constant of 23.1 V after 30,000 contact-separation cycles, indicating excellent mechanical robustness and reliability.

Washability is also a primary demand for wearable electronics in their practical applications. In this work, we created a simulative laundering condition in the presence of household laundry detergents under magnetic stirring (Fig. S15).[29] After 10 times of washing, the electrical performance of NPE-TENG including V_{oc}, I_{sc}, and Q_{sc} can maintain constant at 23.3 V, 0.9 μA, and 7.5 nC, respectively, indicating good washability (Fig. S16a-c). In daily life, wearable electronics will be inevitably exposed to multiple contaminants. It is highly desired for wearable electronics to maintain good electrical output stability when they are contaminated. Therefore, the electrical performances of our NPE-TENG were also conducted after stained with different contaminants, such as milk, olive oil, and dust (Fig. S17). A pristine NPE-TENG can deliver electrical outputs with V_{oc} of 23.5 V, I_{sc} of 0.8 μA, and Q_{sc} of 7.4 nC, respectively (Fig. S16d-f). Because electric generation is determined by the inner NPE@SPNYs dielectric core, when the outer surface of PDMS sheath is polluted by various contaminants, the V_{oc}, I_{sc}, and Q_{sc} of NPE-TENG remain well without obvious degradation, indicating good electrical output stability (Fig. S16d-f). The desirable washing durability and electrical output stability of NPE-TENG can be ascribed to the

steady material property of NPE@SPNYs core and the good protective effect of PDMS sheath.

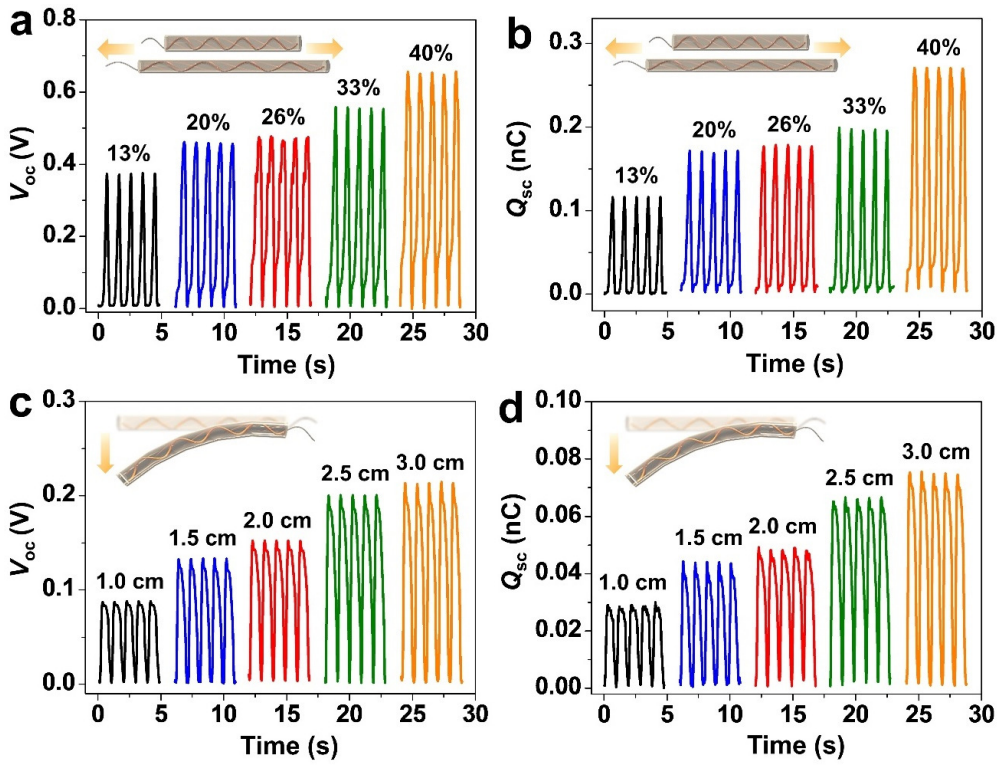

Fig. 3. Electrical performances of NPE-TENG under different mechanical energy harvesting patterns. (a) V_{oc} and (b) Q_{sc} of NPE-TENG under the stretching operation (strain:13 – 40%). (c) V_{oc} and (d) Q_{sc} of NPE-TENG under the bending operation (deflection of 1.0 – 3.0 cm). Insets: Illustrations of NPE-TENG under corresponding mechanical stimuli. Frequency: 1 Hz.

In addition to the compression test, mechanical energy harvesting capacities of our NPE-TENG were also tested under stretching, bending, and twisting to investigate diverse working conditions. In Fig. 3a and 3b, when the stretch strain raises from 13% to 40%, NPE-TENG reveals an obvious enhancement in V_{oc} from 0.38 to 0.66 V and

Q_{sc} from 0.12 to 0.27 nC, respectively. Similarly, the V_{oc} increases distinctly from 0.09 to 0.21 V and the Q_{sc} raises dramatically from 0.029 to 0.076 nC when the extent of bending deflection changes from 1.0 to 3.0 cm (Fig. 3c and 3d). Moreover, when our NPE-TENG is twisted by 90° to 360°, the V_{oc} increases from 1.05 to 2.62 V and the Q_{sc} raises from 0.43 to 0.88 nC (Fig. S18). The helical NPE@SPNYs core structure can provide adequate contact-separation operation space for NPE-TENG. When diverse mechanical stimuli are conducted, such as compressing, stretching, bending, and twisting, the gap size between the NPE@SPNYs core and the PDMS sheath will decrease gradually, thus generate enhanced electrical outputs. The V_{oc} and Q_{sc} of NPE-TENG under the compressing are much higher than that under other mechanical stimuli because the compressing operation may result in a much higher extent of gap size shrinkage than other cases. Energy conversion under diverse deformations not only endow our NPE-TENG with efficient mechanical energy harvesting abilities but also help to broaden the scope of personal health monitoring.

Based on the excellent flexibility and good electrical outputs of our NPE-TENG, a self-powered wearable sensor is developed to monitor different physiological signals and human body activities in a rapid, real-time, highly sensitive, and noninvasive way. Thanks to diverse mechanical deformations, our NPE-TENG can be conformably attached to different positions of a wearer for human body motions sensing (Fig. S19). It is worth noting that the NPE-TENG is coupled with an external resistance of 1 GΩ to maintain its output stability. As a typical subtle expression, blinking is not only an

intuitive channel for expressing emotions, but also the primary external communication platform for paralysis patients. When the NPE-TENG is stuck on the eyelid, alternating blinking activities can be easily monitored by voltage output signals (Fig. 4a). Moreover, a representative blinking waveform is extracted, that is, eyes closing and opening state, which cause an increasing and decreasing pulse signal, respectively. Respiration is a main vital sign that assists to evaluate personal physical condition such as mood change and sleep quality, which can be reflected via the flow of breath. By sticking the NPE-TENG on the vent of a commercial mask, the repeatable voltage signal variations generated by nasal breathing are recorded (Fig. 4b). A regular voltage waveform of breathing with two characteristic peaks is demonstrated, which is related to inhalation and exhalation. In addition, throat-related activities and vocal cord vibrations can be also reflected by the real-time voltage signals of the NPE-TENG. Each specific throat-related activity, such as swallowing, drinking, and coughing, can generate a feature waveform with good regularity and repeatability (colored shadow marks) for easy recognition (Fig. 4c). Moreover, voice recognition can be realized by sticking the NPE-TENG on the throat of a wearer. As expected, random speaking will generate a consecutively random voltage output signal (Fig. S20). Interestingly, the real-time voltage output signals with regular, steady, repeatable, and patterned feature peaks can be recorded when a wearer speaks some specific words or phrases, such as “energy”, “energy harvesting” “fiber” and “nano” (Fig. 4d and S21). More importantly, a word, such as “energy”, can exhibit a consistent voltage characteristic waveform with its extended phrase (“energy harvesting”) (Fig. 4e), showing good reliability and

reproducibility for voice recognition. The voice recognition property of our NPE-TENG is possibly helpful for people with vocal cord diseases to rebuild their speaking ability through the practice of throat muscle activities, which is also capable of facilitating the realization of long-range controlled human-computer interaction.

In addition to tactile detections of skin-level, our NPE-TENG also reveals an excellent response to major joints motions, such as knuckle, elbow, wrist, and knee. By attaching to the elbow, our NPE-TENG can respond to the bending-releasing of the elbow in an angle range from 30° to 120° (Fig. 4f). Each activity is performed seven times, and each curve has a similar voltage characteristic signal, indicating good repeatability for joint-related activities. With the increase of bending angle, the voltage output of NPE-TENG has a gradual enhancement, which is attributed to the increase in the contact area between the elbow and NPE-TENG. Meanwhile, the NPE-TENG can also deliver a stable and repeatable voltage output when it is fixed on the wrist. (Fig. 4g). Moreover, the NPE-TENG is also anchored on the knee of a wearer to further record knee-related motions. In Fig. 4h, the NPE-TENG exhibits diverse amplitudes and frequencies of voltage output waveforms with good repeatability, which can distinguish various knee-related activities including walking, jumping, and jogging. Owing to its good flexibility and high sensitivity under various external mechanical stimuli, our NPE-TENG can be further developed into a self-powered smart glove for gesture detection and recognition. In brief, the smart glove is readily obtained by fixing five NPE-TENG onto the knuckle of a nitrile glove with commercial tape (Fig. S22a). First, real-time voltage signals of

the smart glove were gathered independently via bending five fingers in turn. As shown in Fig. 4i, the smart glove can deliver diverse voltage output waveforms and regular amplitudes with the bending of five fingers from the thumb to the little finger in turn, indicating the excellent capability of gesture detection and recognition. Then, the voltage signals of the smart glove with five NPE-TENG in series were also further collected. The enhanced voltage signals of the smart glove can be easily achieved via controlling the number of bending fingers owning to the enlarged efficient length of NPE-TENG. In Fig. 4j, the voltage output signals of the smart glove can respond to various gestures of a wearer with reproducible waveforms and steady amplitudes. When the wearer makes different gestures, various voltage outputs of the smart glove can be recorded and recognized, such as "Perfect" gesture (~ 2.6 V), "victory" sign (~ 10.5 V), "OK" gesture (~ 12.6 V), and "make a fist" (~ 28.4 V), showing significant potential in high-sensitivity human-machine interactions (Fig. S22b-e and Movie S1 in Supporting Information). Our NPE-TENG shows good tactile sensing capacity, a wide detection range (from physiological signals to joint movements), and stable signal repeatability, which can be compared with the reported TENG-based sensors.[30, 31, 49, 57-59] Based on its reliability and reproducibility, our NPE-TENG is expected to be a promising candidate for robotics and intelligent prosthetics to monitor human movements.

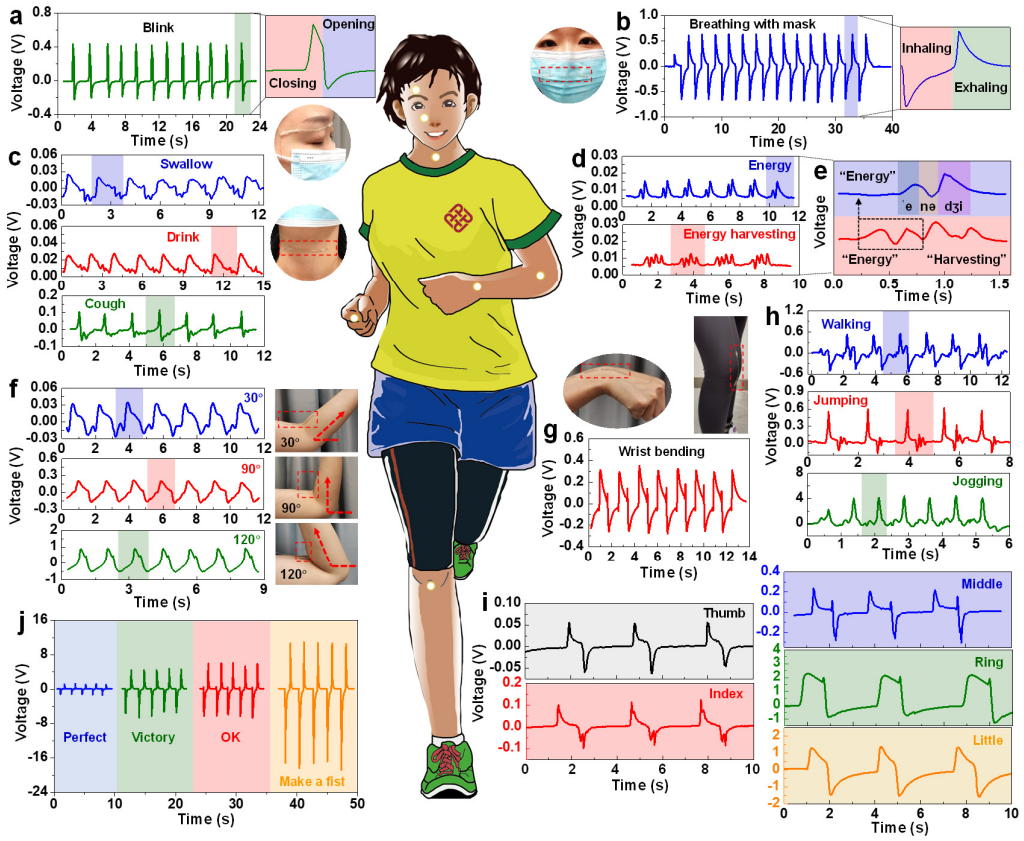

Fig. 4. Applications of NPE-TENG as self-powered wearable sensors and smart glove. (a) Blinking activities detection by pasting NPE-TENG on the eyelid. A complete voltage curve of blinking is enlarged on the right. (b) Nasal breathing sensing by attaching NPE-TENG to a mask. A complete voltage signal of inhaling and exhaling is enlarged on the right. (c) Throat-related activities sensing by pasting NPE-TENG on the throat. (d) Sound recognition by attaching NPE-TENG to a wearer's throat to monitor vocal cord vibrations. (e) A complete waveform of the pronunciation of "energy" and "energy harvesting". (f) Monitoring of elbow bending angles by pasting NPE-TENG on the elbow. (g) Detection of the wrist bending by fixing NPE-TENG on the wrist. (h) Knee-related activities monitoring by attaching NPE-TENG to the knee joint. (i) Real-time voltage signals of the smart glove by bending five fingers in turn. (j) Real-time voltage responses of the smart glove to different gestures.

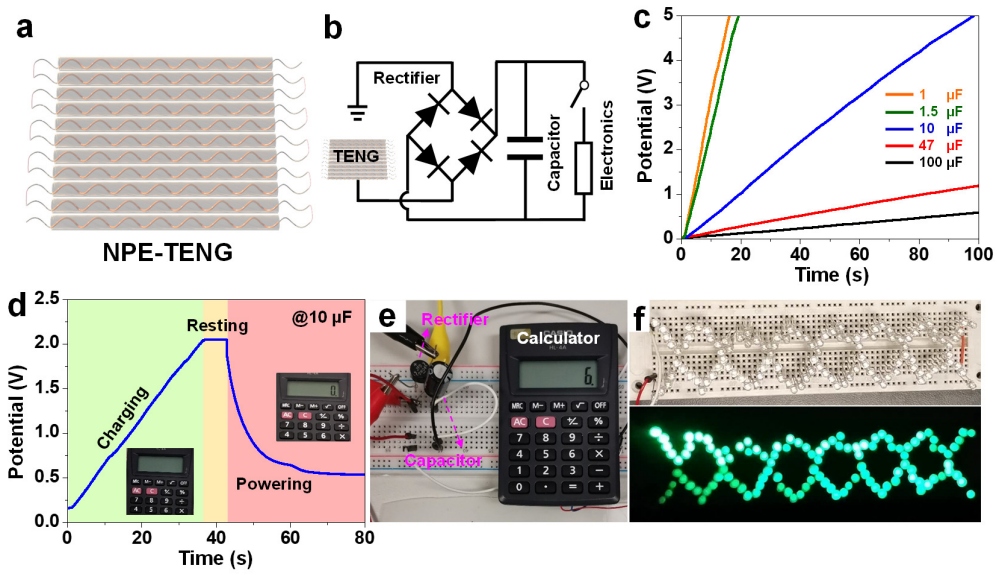

Fig. 5. Energy harvesting applications of twenty NPE-TENG as a power source. (a) Schematic illustration of twenty NPE-TENG in series. (b) The equivalent circuit of charging/discharging of electronics. (c) Charging curves of various capacitors by the NPE-TENG. (d) The charging/discharging curve of a commercial capacitor connected with the NPE-TENG for driving an electrical calculator. (e) The photograph of a calculator powered by the NPE-TENG. (f) 114 green LEDs were directly lighted up by the NPE-TENG.

Apart from versatile sensing applications, our NPE-TENG can perform as a sustainable power source owing to its high electrical outputs. To efficiently drive commercial electronics, twenty NPE-TENG were connected in series (Fig. 5a). Fig. 5b demonstrates the equivalent electrical circuit diagram of a self-powered system including the NPE-TENG as a power source, a capacitor as an energy storage unit, and a rectifier (2W04, ASEMI) as an alternating current-to-direct current converter. The charging curves of capacitors (1, 1.5, 10, 47, and 100 μF) by the NPE-TENG are presented in Fig. 5c. The capacitor of 1, 1.5, and 10 μF can be rapidly charged to 5 V

within 16, 19, and 98 s, respectively. The capacitor of 47 and 100 μF has a charging rate of ~ 120 and ~ 62 mV/s, which is compared with reported fiber-based TENGs.[29-31, 47, 50] Moreover, a self-powered system integrated with NPE-TENG and a 10 μF capacitor can drive an electrical calculator to operate normally (Fig. 5d, 5e and Movie S2 in Supporting Information). As shown in Fig. 5d, the charging voltage of the capacitor raises to 2 V within 35 s rapidly, and then the calculator is successfully driven for ~ 10 s. Additionally, the NPE-TENG can serve as a sustainable power supply and directly light up 114 green LEDs (Fig. 5f and Movie S3 in Supporting Information). The results show our NPE-TENG is very promising as an efficient and clean power source.

3. Conclusion

In summary, we have prepared a kind of nanocomposite polymer electrolytes (NPEs) composed of polycation-modified carbon dots (PCDs) nanofillers and the PVA matrix. The prepared NPEs possessed improved ionic conductivities owing to the contribution of PCDs. Thanks to its enhanced ionic conductivity, a novel NPEs-based fiber triboelectric nanogenerator (NPE-TENG) was proposed and developed for the first time, in which a helical NPEs@SPNYs dielectric core was inserted into the PDMS sheath as dominating triboelectric materials. The assembled NPE-TENG had good flexibility and high electrical outputs under different mechanical stimuli, such as compressing, stretching, bending, and twisting. More importantly, the NPE-TENG had a considerable power density of 265.8 μW m^{-1} and long-term stability of 30,000 cycles. Moreover,

good washability and stain-resistant endowed NPE-TENG with application potential in daily life. In addition, a self-powered wearable sensor based on NPE-TENG was further designed and used to realize the full-range monitoring of physiological signals and joint motions in a rapid, real-time, and noninvasive manner. Meanwhile, a smart glove was also developed for the detection and recognition of different gestures. Finally, the NPE-TENG also performed as a sustainable power source for charging various capacitors, driving small electronics, and lighting up hundreds of LEDs. In the future, the NPE-TENG may play a useful role in human-machine interaction and personal healthcare monitoring.

4. Experimental section

4.1. Preparation of NPE@SPNYs fiber

The preparation of NPE@SPNYs dielectric fiber was divided into the following steps. The first step is to synthesize PCDs for polyelectrolyte nanofillers.[39] Citric acid (CA, 99.5%, Aladdin, 0.2 g), urea (99.5%, Aladdin, 0.5 g) and branched PEI (99%, M.W. = 10,000, Aladdin, 0.01 g/ml) were dissolved in 10 mL Milli-Q water under vigorous stirring. The as-prepared mixture was heated for 5 min in a domestic microwave oven (700 W, Midea, China). After cooling to room temperature, the obtained products were re-dissolved in Milli-Q water and centrifuged at 12,000 rpm for 30 min to remove large carbon residuals. The supernatant solution was further dialyzed against Milli-Q water using a dialysis membrane (MWCO = 50 kDa) for 3 days. Finally, the purified aqueous

solution was lyophilized to obtain brownish polyelectrolyte nanofillers. The second step is to prepare NPEs@SPNYs fiber. PVA (88% hydrolyzed, M.W. 120,000, Acros Organics, 0.2 g/ml) and PCDs (1 wt%, 3 wt%, and 5 wt%) were added to 10 ml Milli-Q water by stirring vigorously under 80 °C for 6 h to obtain a uniform mixture, namely PCDs/PVA NPEs. After cooling naturally, NPEs were coated onto conductive silver-plated nylon yarns (SPNYs, 150 denier, from Qingdao Zhiyuanxiangyu Functional Fabrics Co., Ltd) by dip-coating for several times, and then the prepared fiber was enwound on a stainless-steel rod (SSR) and kept in an oven at 80 °C for 4 h to obtain the helical NPE@SPNYs core fiber.

4.2. Fabrication of core-sheath NPE-TENG

NPE-TENG was fabricated with an NPE@SPNYs dielectric fiber as core and a PDMS tube as sheath. PDMS (Sylgard 184, Dow Corning) and an SSR were selected to prepare PDMS tubes. Firstly, PDMS solution was prepared by mixing the monomer and curing agent in a mass ratio of 10:1 and degassed in a vacuum for 30 min to remove bubbles. Secondly, SSR with a diameter of 1.5 mm was immersed in the mixture and then pulled out slowly. Subsequently, the PDMS-coated SSR was dried in an oven at 80 °C for 2 h and immersed into acetone solutions for 1 h, and then the PDMS tube with an inner diameter of 1.5 mm could be easily peeled off from SSR. Finally, the prepared NPE@SPNYs helical core fiber was inserted into the PDMS sheath tube, and both ends of the tube were encapsulated with PDMS to fabricate the core-sheath structural NPE-TENG.

4.3. Characterization and evaluation

The morphologies of samples were characterized by a scanning electron microscope (SEM, Hitachi TM-3000, Japan). Transmission electron microscopy (TEM) was recorded on Tecnai G2 F20 (FEI Company). Atomic force microscopy image (AFM) was carried out on MFP-3D Infinity (OXFORD instruments). The X-ray diffraction (XRD) pattern was performed on a Bruker X-ray diffractometer (D8 Advance) with Cu Kα radiation. X-ray photoelectron spectroscopy (XPS) spectra were recorded on an ESCALAB210 spectrometer. Fourier transform infrared (FTIR) absorption spectra were carried out on a Perkin Elmer spectrometer (Spectrum 100). Electrical performances of TENG under different applied forces and frequencies were evaluated by a button/key durability life test machine (ZX-A03, Zhongxingda, Shenzhen) equipped with a high speed self-configuring digital indicator (Interface 9860). The open-circuit voltage, short-circuit current and short-circuit charge transfer were recorded by an electrometer (Keithley 6514, Tektronix). Motion monitoring was carried out with assistance of a volunteer (one of authors of this article). The study was approved by the Human Subjects Ethics Sub-committee of Hong Kong Polytechnic University and informed written consent was also obtained from the volunteer. Tensile/compression measurements were performed on a universal tensile testing machine (Instron 4411) equipped with a 5 kN load cell. Electrochemical impedance spectroscopy (EIS) was measured via an electrochemical workstation (Princeton Versa STAT 3) in the frequency range of 100 kHz to 0.01 Hz.

Acknowledgements

The authors would like to acknowledge the funding support from Research Institute of Intelligent Wearable Systems (RI-IWEAR) of The Hong Kong Polytechnic University (1-CD43) for the work reported here.

References

[1] J. Xiong, P. Cui, X. Chen, J. Wang, K. Parida, M.-F. Lin, P. S. Lee, *Nat. Commun.* **2018**, *9*, 4280.

[2] J. Tu, R. M. Torrente-Rodríguez, M. Wang, W. Gao, *Adv. Funct. Mater.* **2020**, *30*, 1906713.

[3] J. Kim, A. S. Campbell, B. E.-F. de Ávila, J. Wang, *Nat. Biotechnol.* **2019**, *37*, 389.

[4] A. M. Zamarayeva, A. E. Ostfeld, M. Wang, J. K. Duey, I. Deckman, B. P. Lechêne, G. Davies, D. A. Steingart, A. C. Arias, *Sci. Adv.* **2017**, *3*, e1602051.

[5] D. Bogdanov, J. Farfan, K. Sadovskaia, A. Aghahosseini, M. Child, A. Gulagi, A. S. Oyewo, L. de Souza Noel Simas Barbosa, C. Breyer, *Nat. Commun.* **2019**, *10*, 1077.

[6] W. Zuo, R. Li, C. Zhou, Y. Li, J. Xia, J. Liu, *Adv. Sci.* **2017**, *4*, 1600539.

[7] H. Tang, J. Yao, Y. Zhu, *Adv. Energy Mater.* **2021**, *11*, 2003994.

[8] H. Zhang, X. Liu, H. Li, I. Hasa, S. Passerini, *Angew. Chem. Int. Edit.* **2021**, *60*, 598.

[9] Y. Liang, C.-Z. Zhao, H. Yuan, Y. Chen, W. Zhang, J.-Q. Huang, D. Yu, Y. Liu, M.-M. Titirici, Y.-L. Chueh, H. Yu, Q. Zhang, *InfoMat* **2019**, *1*, 6.

[10] P. K. Nayak, S. Mahesh, H. J. Snaith, D. Cahen, *Nat. Rev. Mater.* **2019**, *4*, 269.

[11] I. Chung, B. Lee, J. He, R. P. H. Chang, M. G. Kanatzidis, *Nature* **2012**, *485*, 486.

[12] G. Wang, F. S. Melkonyan, A. Facchetti, T. J. Marks, *Angew. Chem. Int. Edit.* **2019**, *58*, 4129.

[13] M. Haras, T. Skotnicki, *Nano Energy* **2018**, *54*, 461.

[14] S. Hong, Y. Gu, J. K. Seo, J. Wang, P. Liu, Y. S. Meng, S. Xu, R. Chen, *Sci. Adv.* **2019**, *5*, eaaw0536.

[15] C.-e. Zhao, P. Gai, R. Song, Y. Chen, J. Zhang, J.-J. Zhu, *Chem. Soc. Rev.* **2017**, *46*, 1545.

[16] T. R. Ray, J. Choi, A. J. Bandodkar, S. Krishnan, P. Gutruf, L. Tian, R. Ghaffari, J. A. Rogers, *Chem. Rev.* **2019**, *119*, 5461.

[17] Z. L. Wang, A. C. Wang, *Mater. Today* **2019**, *30*, 34.

[18] Z. L. Wang, J. Chen, L. Lin, *Energy Environ. Sci.* **2015**, *8*, 2250.

[19] J. Luo, Z. L. Wang, *Energy Storage Mater.* **2019**, *23*, 617.

[20] Y. Zhou, M. Shen, X. Cui, Y. Shao, L. Li, Y. Zhang, *Nano Energy* **2021**, *84*, 105887.

[21] X. Pu, S. An, Q. Tang, H. Guo, C. Hu, *iScience* **2021**, *24*, 102027.

[22] F. Yi, Z. Zhang, Z. Kang, Q. Liao, Y. Zhang, *Adv. Funct. Mater.* **2019**, *29*, 1808849.

[23] X. Chen, X. Xie, Y. Liu, C. Zhao, M. Wen, Z. Wen, *Adv. Funct. Mater.* **2020**, *30*, 2004673.

[24] K. Dong, X. Peng, Z. L. Wang, *Adv. Mater.* **2020**, *32*, 1902549.

[25] Y. Hu, Z. Zheng, *Nano Energy* **2019**, *56*, 16.

[26] L. Huang, S. Lin, Z. Xu, H. Zhou, J. Duan, B. Hu, J. Zhou, *Adv. Mater.* **2020**, *32*, 1902034.

[27] S. J. Varma, K. Sambath Kumar, S. Seal, S. Rajaraman, J. Thomas, *Adv. Sci.* **2018**, *5*, 1800340.

[28] K. Dong, J. Deng, W. Ding, A. C. Wang, P. Wang, C. Cheng, Y.-C. Wang, L. Jin, B. Gu, B. Sun, Z. L. Wang, *Adv. Energy Mater.* **2018**, *8*, 1801114.

[29] K. Dong, X. Peng, J. An, A. C. Wang, J. Luo, B. Sun, J. Wang, Z. L. Wang, *Nat. Commun.* **2020**, *11*, 2868.

[30] J. Han, C. Xu, J. Zhang, N. Xu, Y. Xiong, X. Cao, Y. Liang, L. Zheng, J. Sun, J. Zhai, Q. Sun, Z. L. Wang, *ACS Nano* **2021**, *15*, 1597.

[31] C. Ning, K. Dong, R. Cheng, J. Yi, C. Ye, X. Peng, F. Sheng, Y. Jiang, Z. L. Wang, *Adv. Funct. Mater.* **2021**, *31*, 2006679.

[32] H. Ryu, J.-H. Lee, T.-Y. Kim, U. Khan, J. H. Lee, S. S. Kwak, H.-J. Yoon, S.-W. Kim, *Adv. Energy Mater.* **2017**, *7*, 1700289.

[33] L. Shi, S. Dong, H. Xu, S. Huang, Q. Ye, S. Liu, T. Wu, J. Chen, S. Zhang, S. Li, X. Wang, H. Jin, J. M. Kim, J. Luo, *Nano Energy* **2019**, *64*, 103960.

[34] R. Ccorahua, J. Huaroto, C. Luyo, M. Quintana, E. A. Vela, *Nano Energy* **2019**, *59*, 610.

[35] R. Wang, L. Mu, Y. Bao, H. Lin, T. Ji, Y. Shi, J. Zhu, W. Wu, *Adv. Mater.* **2020**, *32*, 2002878.

[36] L. Jin, X. Xiao, W. Deng, A. Nashalian, D. He, V. Raveendran, C. Yan, H. Su, X. Chu, T. Yang, W. Li, W. Yang, J. Chen, *Nano Lett.* **2020**, *20*, 6404.

[37] G. J. Choi, S. H. Baek, S. S. Lee, F. Khan, J. H. Kim, I. K. Park, *J. Alloys Compd.* **2019**, *797*, 945.

[38] V. Harnchana, H. V. Ngoc, W. He, A. Rasheed, H. Park, V. Amornkitbamrung, D. J. Kang, *ACS Appl. Mater. Interfaces* **2018**, *10*, 25263.

[39] Z. Li, B. Xu, J. Han, J. Huang, K. Y. Chung, *Adv. Energy Mater.* **2021**, *11*, 2101294.

[40] C. Ma, K. Dai, H. Hou, X. Ji, L. Chen, D. G. Ivey, W. Wei, *Adv. Sci.* **2018**, *5*,

1700996.

[41] Z. Li, F. Liu, S. Chen, F. Zhai, Y. Li, Y. Feng, W. Feng, *Nano Energy* **2021**, *82*, 105698.

[42] D. Lin, W. Liu, Y. Liu, H. R. Lee, P.-C. Hsu, K. Liu, Y. Cui, *Nano Lett.* **2016**, *16*, 459.

[43] Y. Hu, W. Chen, T. Lei, B. Zhou, Y. Jiao, Y. Yan, X. Du, J. Huang, C. Wu, X. Wang, Y. Wang, B. Chen, J. Xu, C. Wang, J. Xiong, *Adv. Energy Mater.* **2019**, *9*, 1802955.

[44] W. Bu, X. Xu, Z. Wang, N. Jin, L. Liu, J. Liu, S. Zhu, K. Zhang, R. Jelinek, D. Zhou, H. Sun, B. Yang, *ACS Appl. Mater. Interfaces* **2020**, *12*, 50287.

[45] X. Chen, A. Yusuf, J. S. del Rio, D. Y. Wang, *Nano Energy* **2021**, *81*, 105656.

[46] H. Li, C. Han, Y. Huang, Y. Huang, M. Zhu, Z. Pei, Q. Xue, Z. Wang, Z. Liu, Z. Tang, Y. Wang, F. Kang, B. Li, C. Zhi, *Energy Environ. Sci.* **2018**, *11*, 941.

[47] L. Xie, X. Chen, Z. Wen, Y. Yang, J. Shi, C. Chen, M. Peng, Y. Liu, X. Sun, *Nano-Micro Lett.* **2019**, *11*, 39.

[48] Y. Yang, L. Xie, Z. Wen, C. Chen, X. Chen, A. Wei, P. Cheng, X. Xie, X. Sun, *ACS Appl. Mater. Interfaces* **2018**, *10*, 42356.

[49] Y. Cheng, X. Lu, K. Hoe Chan, R. Wang, Z. Cao, J. Sun, G. Wei Ho, *Nano Energy* **2017**, *41*, 511.

[50] X. He, Y. Zi, H. Guo, H. Zheng, Y. Xi, C. Wu, J. Wang, W. Zhang, C. Lu, Z. L. Wang, *Adv. Funct. Mater.* **2017**, *27*, 1604378.

[51] K. Dong, J. Deng, Y. Zi, Y.-C. Wang, C. Xu, H. Zou, W. Ding, Y. Dai, B. Gu, B. Sun, Z. L. Wang, *Adv. Mater.* **2017**, *29*, 1702648.

[52] N. Wang, Y. Feng, Y. Zheng, L. Zhang, M. Feng, X. Li, F. Zhou, D. Wang, *Adv. Funct. Mater.* **2021**, *31*, 2009172.

[53] L. S. McCarty, G. M. Whitesides, *Angew. Chem. Int. Edit.* **2008**, *47*, 2188.

[54] S. Wang, L. Lin, Z. L. Wang, *Nano Lett.* **2012**, *12*, 6339.

[55] J. Shen, Z. Li, J. Yu, B. Ding, *Nano Energy* **2017**, *40*, 282.

[56] X.-S. Zhang, M.-D. Han, R.-X. Wang, F.-Y. Zhu, Z.-H. Li, W. Wang, H.-X. Zhang, *Nano Lett.* **2013**, *13*, 1168.

[57] M. Zhu, M. Lou, J. Yu, Z. Li, B. Ding, *Nano Energy* **2020**, *78*, 105208.

[58] X. Peng, K. Dong, C. Ye, Y. Jiang, S. Zhai, R. Cheng, D. Liu, X. Gao, J. Wang, Z. L. Wang, *Sci. Adv.* **2020**, *6*, 9624.

[59] K. Dong, Z. Wu, J. Deng, A. C. Wang, H. Zou, C. Chen, D. Hu, B. Gu, B. Sun, Z. L. Wang, *Adv. Mater.* **2018**, *30*, 1804944.